

Precise Mono-Selective Aromatic C-H Bond Activation by Chemisorption of Meta-Aryne on a Metal Surface

Qitang Fan, Simon Werner, Jalmar Tschakert, Daniel Ebeling, Andre Schirmeisen, Gerhard Hilt, Wolfgang Hieringer, and J. Michael Gottfried

J. Am. Chem. Soc., **Just Accepted Manuscript** • DOI: 10.1021/jacs.8b01658 • Publication Date (Web): 11 May 2018

Downloaded from <http://pubs.acs.org> on May 13, 2018

Just Accepted

“Just Accepted” manuscripts have been peer-reviewed and accepted for publication. They are posted online prior to technical editing, formatting for publication and author proofing. The American Chemical Society provides “Just Accepted” as a service to the research community to expedite the dissemination of scientific material as soon as possible after acceptance. “Just Accepted” manuscripts appear in full in PDF format accompanied by an HTML abstract. “Just Accepted” manuscripts have been fully peer reviewed, but should not be considered the official version of record. They are citable by the Digital Object Identifier (DOI®). “Just Accepted” is an optional service offered to authors. Therefore, the “Just Accepted” Web site may not include all articles that will be published in the journal. After a manuscript is technically edited and formatted, it will be removed from the “Just Accepted” Web site and published as an ASAP article. Note that technical editing may introduce minor changes to the manuscript text and/or graphics which could affect content, and all legal disclaimers and ethical guidelines that apply to the journal pertain. ACS cannot be held responsible for errors or consequences arising from the use of information contained in these “Just Accepted” manuscripts.

Precise Mono-Selective Aromatic C-H Bond Activation by Chemisorption of *Meta*-Aryne on a Metal Surface

Qitang Fan^{†‡}, Simon Werner^{†‡}, Jalmar Tschakert², Daniel Ebeling², André Schirmeisen^{2*}, Gerhard Hilt^{3*}, Wolfgang Hieringer^{4*}, J. Michael Gottfried^{1*}

¹Department of Chemistry, Philipps University Marburg, Hans-Meerwein-Straße 4, 35037 Marburg, Germany

²Institute of Applied Physics (IAP), Justus Liebig University Gießen, Heinrich-Buff-Ring 16, 35392 Gießen, Germany

³Institute of Chemistry, Carl von Ossietzky University Oldenburg, Carl-von-Ossietzky-Straße 9-11, 26111 Oldenburg, Germany

⁴Theoretical Chemistry and Interdisciplinary Center for Molecular Materials (ICMM), Department of Chemistry and Pharmacy, Friedrich-Alexander-Universität Erlangen-Nürnberg, Egerlandstraße 3, 91058 Erlangen, Germany

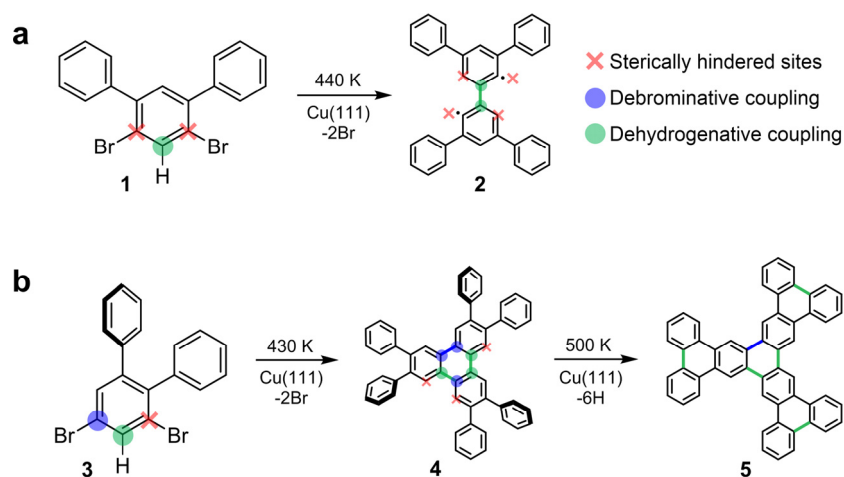
ABSTRACT: Aromatic C-H bond activation has attracted much attention due to its versatile applications in the synthesis of aryl-containing chemicals. The major challenge lies in the minimization of the activation barrier and maximization of the regioselectivity. Here, we report the highly selective activation of the central aromatic C-H bond in *meta*-aryne species anchored to a copper surface, which catalyzes the C-H bond dissociation. Two prototype molecules, *i.e.*, 4',6'-dibromo-*meta*-terphenyl and 3',5'-dibromo-*ortho*-terphenyl have been employed to perform C-C coupling reactions on Cu(111). The chemical structures of the resulting products have been clarified by a combination of scanning tunneling microscopy and non-contact atomic force microscopy. Both methods demonstrate a remarkable weakening of the targeted C-H bond. Density functional theory calculations reveal that this efficient C-H activation stems from the extraordinary chemisorption of the *meta*-aryne on the Cu(111) surface, resulting in the close proximity of the targeted C-H group to the Cu(111) surface and the absence of planarity of the phenyl ring. These effects lead to a lowering of the C-H dissociation barrier from 1.80 eV to 1.13 eV, in agreement with the experimental data.

INTRODUCTION

Aromatic C-H bond functionalization is one of the most efficient and economic approaches for the synthesis of aryl-containing pharmaceuticals, agrochemicals, and modern advanced materials.¹ The necessary activation of the C-H bonds is often achieved by using transition metal catalysts.²⁻⁷ Because of the ubiquity of C-H bonds in aromatic compounds, high regioselectivity of the activation is often required. One of the most successful approaches in solution chemistry is the directing group strategy,⁸⁻⁹ which enables *ortho*, *meta*, or *para* C-H activation with versatile functional groups.¹⁰ For instance, a coordinative directing group could bind to the metal catalyst, which activates two identical *ortho* C-H bonds due to their close proximity.¹¹⁻¹³ Alternative approaches developed recently for selective C-H functionalization include the metal surface-catalyzed dehydrogenative C-C coupling.¹⁴ The on-surface intramolecular cyclodehydrogenation is of high selectivity and has been utilized widely for the synthesis of graphene nanoribbons,¹⁵⁻¹⁸ nanographene,¹⁹⁻²¹ C₆₀,²² and carbon nanotubes.²³ In addition, the intermolecular dehydrogenative coupling has been employed to synthesize zero-, one- and two-dimensional (2D) covalent nanostructures.²⁴⁻³¹ Nevertheless, these in-solution and on-surface approaches generally account for a chemoselective activation of multiple equivalent C-H bonds. Currently, it is still challenging to attain

catalytic regioselectivity, *i.e.*, the specific activation of a single C-H bond in the presence of others.

Here, we report the highly selective activation of C-H bonds (Scheme 1, green spheres) between two *meta*-substituted C-Br groups in the precursor molecules 4',6'-dibromo-*meta*-terphenyl (DBMTP) **1** (Scheme 1) and 3',5'-dibromo-*ortho*-terphenyl (DBTOP) **3** (Scheme 1). Density functional theory (DFT) calculations reveal that the targeted C-H bonds have been significantly weakened due to the chemisorption of the *meta*-aryne species formed upon deposition of the bromo-arenes on the Cu(111) surface. In solution chemistry, it is usually difficult to explore the influence of radicals on the activation of adjacent C-H bonds, because radical recombination and C-C coupling typically occurs prior to the C-H bond scission. In this study, phenyl substituents have been employed to block the Ullmann coupling at the C-Br positions (Scheme 1, red crosses) in the 2D confinement of the Cu(111) surface. As shown by Scheme 1, DBMTP, with two C-Br positions blocked from debrominative coupling, undergoes exclusively dehydrogenative C-C coupling into the 5',5''-diphenyl-*meta*-quaterphenyl biradical (DMQBR) **2**. The DBOTP, with one



Scheme 1. Reaction of (a) 4',6'-dibromo-*meta*-terphenyl (DBMTP) **1** and (b) 3',5'-dibromo-*ortho*-terphenyl (DBOTP) **3** into the dimer 5',5''-diphenyl-*meta*-quaterphenyl biradical (DMQBR) **2** and trimer 2,3,6,7,10,11-hexaphenyl-triphenylene (HPTP) **4**, respectively. Further cyclodehydrogenation of **4** leads to the formation of hexabenzotrinitriaphthylene (HBTN) **5**. Note that **2**, **4** and **5** are the products formed by assuming that all of the hydrogen atoms from the C-H scission are transferred to neighboring carbon radical sites (see text for details). The displayed *anti* configuration of the radical centers in compound **2** is more stable (by 0.5 eV) than the corresponding *syn* configuration, as revealed by DFT calculations (see Figure S12 in the SI).

blocked C-Br position, forms 2,3,6,7,10,11-hexaphenyl-triphenylene (HPTP) **4** via C-C coupling at one debrominated and one dehydrogenated carbon position. These structures and the high yields of the products have been clarified unambiguously by a combination of scanning tunneling microscopy (STM) and non-contact atomic force microscopy (nc-AFM).

RESULTS AND DISCUSSION

Deposition of a submonolayer of DBMTP onto a Cu(111) surface at 300 K followed by annealing to 400 K results in the formation of well-ordered islands with hexagonally arranged pores, as shown in Figure 1a. The detailed structure of the upper-right island is revealed by the magnified STM image (Figure 1b) of the white-framed region in Figure 1a. As can be seen, each pore is surrounded by six wing-shaped motifs rotated by multiples of 60°, in a clockwise (CW) manner. These wing-shaped motifs are attributed to debrominated *meta*-terphenyl (MTP) biradicals, as shown by the molecular structures in Figure 1c (or that overlaid in Figure 1b). The weak protrusions between the MTP biradicals (as marked by yellow dots in Figure 1b) are attributed to bromine adatoms. They result from C-Br bond scission and form hydrogen bonds with the peripheral hydrogen atoms of the MTP biradicals for the stabilization of the island, as similarly observed in previous work.³²⁻³³ These assignments are supported by the following aspects: First, dissociation of aryl C-Br bonds is complete already below 240 K on Cu(111), according to previous studies,³²⁻³⁴⁻³⁶ which excludes the possibility that the motifs are intact DBMTP. Second, the width of the wing-shaped motif, according to Figure 1b, is 9.6 ± 0.3 Å, in agreement with the size of the MTP radical (9.7 Å) in previous work.³⁵ Third, the absence of protrusion features connected to the two carbon radical ends of the MTP motifs indicates that they bind to substrate lattice copper atoms rather than to copper adatoms

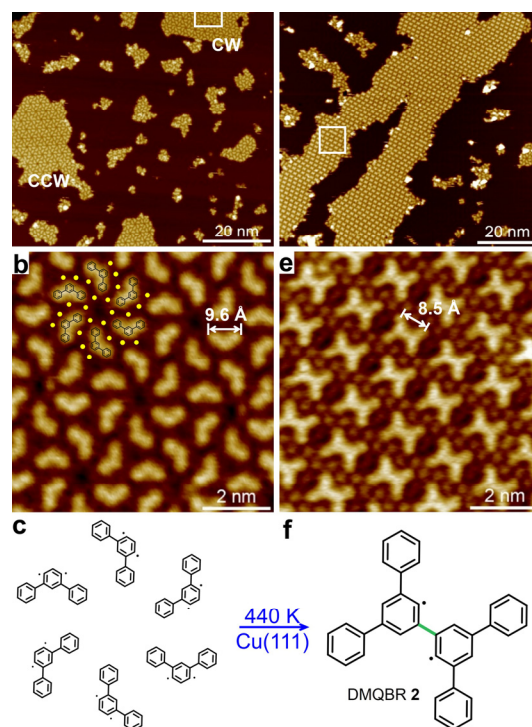


Figure 1. STM images taken after deposition of a submonolayer of DBMTP onto Cu(111) at 300 K, followed by annealing to (a) 400 K and (d) 440 K. Panels (b) and (e) show the magnified views of the white-framed regions in panel (a) and (d), respectively. Molecular structures are overlaid on panel (b). The yellow spheres in panel (b) denote Br adatoms. Panels (c) and (f) show the molecular structures of the species shown in panels (b) and (e), respectively. The sizes and mutual distances of the molecular structures in (c) are in accordance with the STM image in (b). Tunneling parameters for all images: $I = 0.12$ nA, $U = -3.2$ V.

(see the comparison with C-Cu-C linked MTP dimers in Figure S1 in the SI).³⁷ This case is qualitatively very similar to the previously reported adsorption of aromatic radicals on metal surfaces.³⁸⁻⁴² Moreover, the distances between the radical carbon and the neighboring bromine atoms are too short to allow the bonding of a Cu atom to the radical carbon (see the detailed analysis in Figure S2 in the SI). Noteworthy, besides the domains with clockwise (CW) arranged MTP biradicals, the corresponding enantiomeric domains with counterclockwise (CCW) arrangement can also be seen in Figure 1a.

Further annealing to 440 K transforms the MTP biradicals in Figure 1a into a new species, which forms islands as shown in Figure 1d. The zoom-in STM image of the island (Figure 1e) reveals that this species is composed of two back-to-back linked wing-shaped motifs. The experimental distance (8.5 ± 0.3 Å, marked in Figure 1e) between the terminals of the two wings indicates that they are linked by a C-C covalent bond. (For a detailed bond assignment analysis, see Figure S3 in the SI). This butterfly-shaped species is therefore identified as the covalently

linked dimer of MTP units, *i.e.*, the 5',5''-diphenyl-*meta*-quaterphenyl biradical (DMQBR) **2**, as illustrated by the molecular model in Figure 1f. This implies that two DBMTP precursors undergo dehydrogenative coupling at the C-H position between two former C-Br positions, as illustrated in Scheme 1a. The high yield (89 ± 3 %, see Figure S4 in the SI for statistical data) of the newly formed DMQBR molecules thus indicates the highly selective activation of the target C-H bond over the others. Note that the assignment of the butterfly-shaped species as a biradical is based on the assumption that the hydrogen atoms released by the C-H scission are transferred to the neighboring, formerly brominated radicalic carbons, either *via* a hydrogen atom dissociation-association sequence or by an intramolecular 1,2-hydrogen shift. Annealing of DMQBR molecules to higher temperatures (480 K) leads to further dehydrogenation and formation of intramolecular C-C bonds (see detailed discussion in the SI, Figure S5). The fact that higher temperatures are needed for the activation of the other C-H bonds demonstrates the considerable weakening of the target C-H bond.

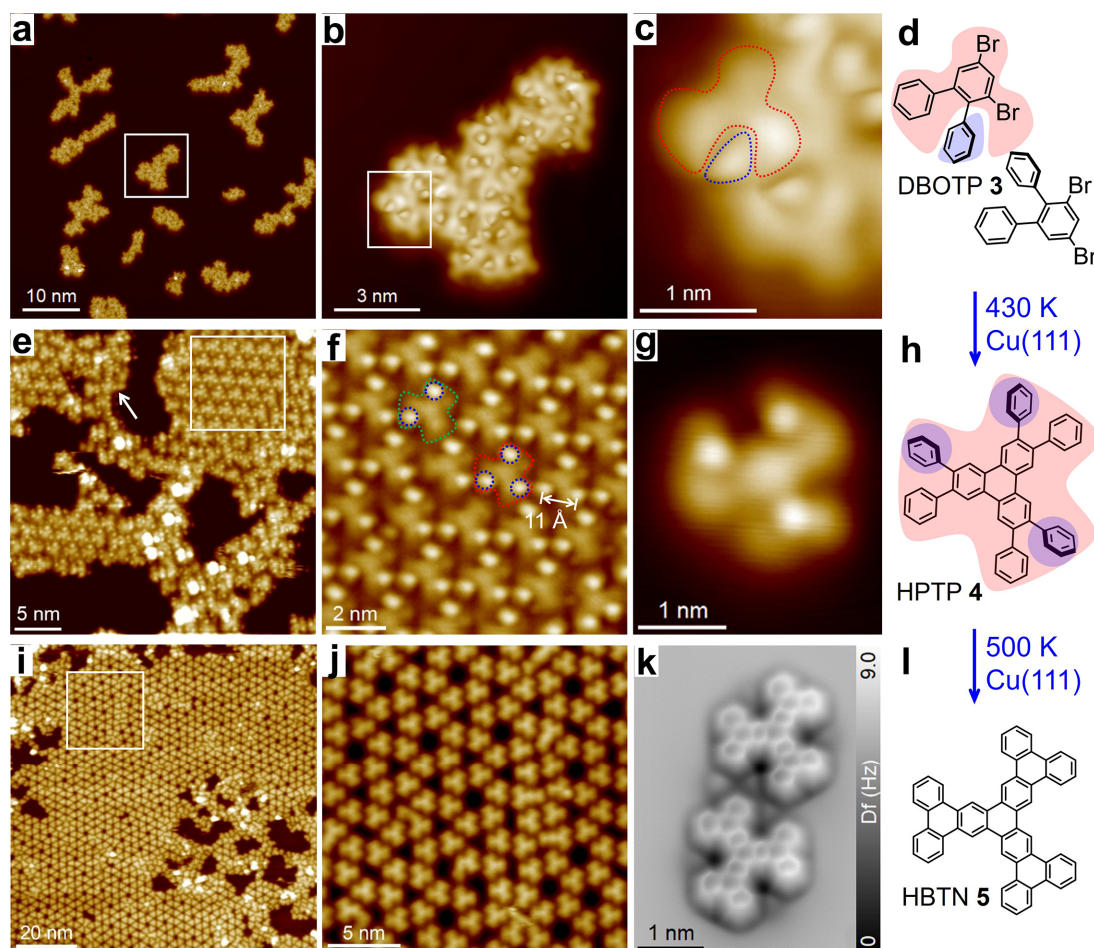


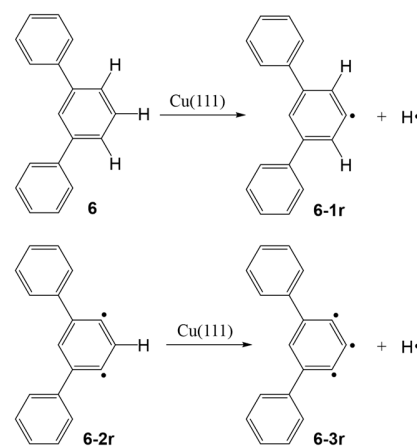
Figure 2. STM images taken after deposition of a submonolayer of DBOTP **3** onto Cu(111) at (a) <math><100\text{ K}</math> and (e) 430 K. Image (i) was taken after annealing the sample in panel (e) to 500 K. Panels (b),(f),(j) show the magnified views of the white-framed regions in panels (a), (e), and (i), respectively. Panels (c), (g) and (k) show the submolecularly resolved STM or nc-AFM images of the species in panels (b), (f), and (j), respectively. Panels (d), (h), (i) show the molecular structures of the species in panels (c), (g), and (k), respectively. Tunneling parameters: (a), (b), (c) $I = 0.01\text{ nA}$, $U = 0.10\text{ V}$; (e), (f) $I = 0.11\text{ nA}$, $U = 1.96\text{ V}$; (g) $I = 0.1\text{ nA}$, $U = -2.02\text{ V}$; (i), (j) $I = 0.05\text{ nA}$, $U = 1.90\text{ V}$; (k) $I = 0.15\text{ nA}$, $U = -0.50\text{ V}$.

To further demonstrate the potential of this effective C-H activation by *meta*-aryne chemisorption, 3',5'-dibromo-*ortho*-terphenyl (DBOTP) **3** has been employed. In this molecule, only one of the two C-Br positions is blocked from the Ullmann coupling by an adjacent phenyl ring. As a result, we expect DBOTP to engage in a combination of debrominative (Ullmann-type) and dehydrogenative C-C coupling, as is discussed below. Because of the less symmetric structure of this precursor and its more complex reaction, a more detailed structural analysis is necessary. The deposition of a submonolayer of DBOTP onto Cu(111) at < 100 K results in the formation of dendritic islands as shown in Figure 2a. These islands have a disordered internal structure. This can be seen in Figure 2b, which shows a magnified view of the white-framed island in Figure 2a (see also the related nc-AFM image in Figure S6 in the SI). Careful inspection of the topography reveals that this structure is composed of uniform four-lobed motifs. In Figure 2c, which shows the zoom-in image of the white-framed region in Figure 2b, one of these motifs is marked with contours (dotted curves). Considering the relative positions and apparent heights of the four lobes, the part marked by the red dotted curve is assigned to the two peripheral phenyl groups and the two bromine atoms in the intact DBOTP molecule, as illustrated by the molecular structure (red shaded part) in Figure 2d. This assignment is supported by the following two observations: First, the X-ray photoemission (XP) spectra indicate that the DBOTP molecules **3** stay intact on Cu(111) below 160 K (Figure S7). Second, the fourth lobe, marked by the blue line in Figure 2c, has a sharper edge and larger apparent height. This feature is attributed to a phenyl ring that is tilted relative to the surface plane for steric reasons. In Figure 2d, this phenyl group is blue shaded. Noteworthy, the DBOTP molecule **3** has two enantiomeric adsorption configurations due to its asymmetric molecular structure. Both enantiomers are shown in Figure 2c and 2d.

Increasing the surface temperature to 430 K during the deposition of DBOTP **3** results predominantly in the formation of ordered islands with a hexagonally close-packed pattern, as shown in Figure 2e. Figure 2f displays a magnified view of these islands, which consist of three-lobed "clover"-like motifs as outlined by the red dotted curve. The majority of these motifs have a three-fold rotational symmetry and each lobe contains one bright spot (marked with blue dotted circles in Figure 2f). This three-fold symmetric trimer species is identified as 2,3,6,7,10,11-hexaphenyl-triphenylene⁴³ (HPTP) **4** consisting of three covalently linked OTP (*ortho*-terphenyl) units. The following findings support this assignment: First, the profile of each lobe in the trimer species resembles the OTP moiety in intact DBOTP (see Figure 2c). This includes the bright spot in each lobe, which is attributed to the tilted phenyl group in an OTP moiety. Second, the measured distance of 11 ± 0.3 Å between two bright spots agrees well with the distance between two tilting phenyl groups in HPTP (Scheme 1, **4**). Third, the evolution of HPTP into a completely flat trimer species, as will be discussed below, further confirms the proposed molecular structure.

The HPTP molecule has multiple adsorption configurations on Cu(111) due to the different relative locations and tilting modes of the phenyl groups in each OTP lobe. For instance, the HPTP molecule in Figure 2g (the corresponding molecular structure is shown in Figure 2h) contains three tilted phenyl groups (blue shaded) with relative positions different from those in the HPTP molecule in Figure 2f (marked with the red dotted curve, tilted phenyls marked by blue circles). Such absence of three-fold symmetry of HPTP **4** molecules on Cu(111) accounts for their partial aggregation into disordered islands, as can be seen in Figure 2e (marked with white arrow). Regardless of the different adsorption configurations, the total yield of the formed HPTP molecules is up to $86 \pm 5\%$ according to the statistics obtained from large-scale STM images of the sample (see Figure S8). The HPTP molecules are formed by the cyclic trimerization of DBOTP monomers, which is achieved by intermolecular Ullmann-type C-C coupling involving the non-hindered C-Br positions (Scheme 1, blue sphere) and the C-H positions (Scheme 1, green sphere). The remaining, sterically hindered former C-Br position has been blocked from C-C coupling by the outer two *ortho*-substituted phenyl groups. Therefore, the high yield of HPTP formed from DBOTP again indicates the highly selective activation of the central C-H bond, which is consistent with the findings for DBMTP in our first example.

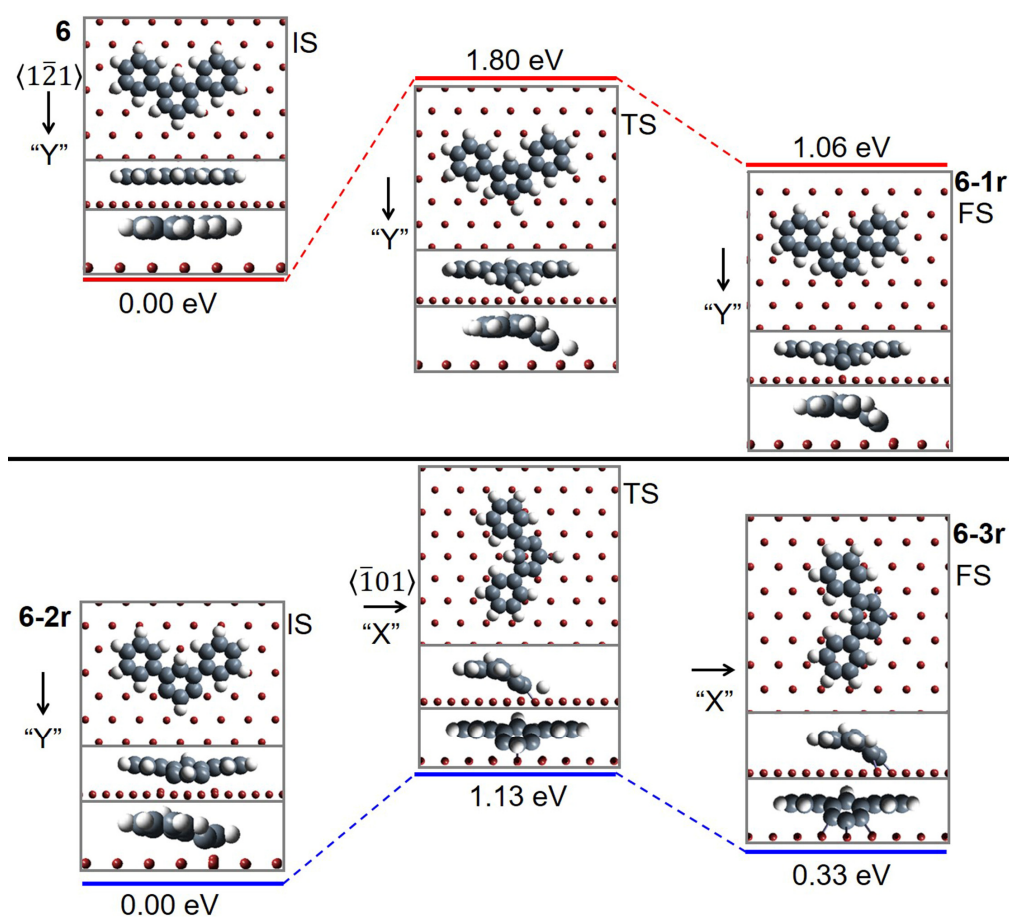
Further annealing of the sample with the HPTP islands in Figure 2e to 500 K leads predominantly to the formation of the porous structure shown in Figure 2i. As revealed by the magnified STM image in Figure 2j, this structure consists of three-fold symmetric molecules with three lobes. Importantly, this species has a uniform apparent height, unlike the HPTP molecules. The detailed molecular structure of this new species has been further clarified by the submolecularly resolved nc-AFM images in Figure 2k (see also the enlarged nc-AFM image in Figure S9 in the SI). In



Scheme 2. C-H activation of 1,1':3',1''-terphenyl **6** and its biradical **6-2r** on Cu(111). The dots symbolize radical positions which bind to Cu atoms of the Cu(111) surface (not shown). See the Tables S1-S3 in the SI for calculated reaction energies and activation barriers using DFT, and Figure S11 for optimized geometries.

1
2
3 this way, the three-lobed species is unambiguously identified as hexabenz[*a,c,k,m,u,w*]trinaphthylene⁴⁴⁻⁴⁵ (HBTN) **5** as shown by the molecular structure in Figure 2i. This implies that the HPTP molecules undergo cyclodehydrogenative C-C coupling at the three OTP moieties around 500 K, forming the flat HBTN molecules consisting of three linked triphenylene moieties. Note that the cyclodehydrogenation of OTP moieties is only occasionally observed at 430 K, as evidenced by the few molecules with one flat lobe (*i.e.*, triphenylene moiety). One example is marked with a green dotted curve in Figure 2f. Annealing the HPTP mol-

To further explore the details of this C-H bond activation, periodic DFT calculations of the *meta*-terphenyl (MTP) *meta*-aryne biradical **6-2r**, formed by C-Br dissociation of DBMTP, and the pristine 1,1':3,1"-terphenyl (TP **6**) on Cu(111) according to Scheme 2 were performed (see the Methods section and the Supporting Information for computational details). Two different adsorption orientations with respect to the underlying Cu(111) surface lattice were considered for the initial (reactant) states (IS, **6**, **6-2r**), transition states (TS), and final (product) states (FS, **6-1r**, **6-3r**) in the C-H activation. These orientations are related



43 Figure 3. The optimized adsorption geometries and energies of the initial states (IS), transition states (TS) and final states (FS) in the C-H activation (with lowest reaction barriers) of **6** and **6-2r**. For the adsorbed species, two different orientations are considered, with the target C-H bond either parallel ("X") or perpendicular ("Y") to a high-symmetric direction of Cu(111). Three different views are given for each adsorbates. Only the molecules and the atoms of the topmost Cu layer are shown. The hydrogen atoms missing in the final states were taken into account through separate calculations of H in a Cu(111) unit cell for the energy calculations. Further geometries and corresponding energies are shown in Figure S11 and Tables S1-S3 in the SI.

49 ecules to 470 K (Figure S10) converted $74 \pm 3\%$ OTP into triphenylene moieties by the cyclodehydrogenation process, which is complete at 500 K, as shown by Figure 2i. Obviously, there is a considerable temperature difference of 70 K between the initial activation of the target C-H bond (green in Scheme 1) and the activation of the other C-H bonds in the cyclodehydrogenation. This implies a non-trivial lowering of the energy barrier for the scission of a C-H bond between two (formerly) brominated positions, as compared to the other C-H bonds.

to each other by 90° rotation around the Cu(111) surface normal. The corresponding optimized geometries of all states are shown in Figure S11 of the Supporting Information along with the corresponding energies provided in Tables S1-S3. The reaction pathways with the lowest effective activation barriers from both orientations are presented in Figure 3. An alternative pathway involving a 1,2-hydrogen shift has a significantly higher activation barrier, as is discussed in the Supporting Information (Scheme S1 and Figure S13).

Intact TP **6** favors adsorption on Cu(111) in **Y** orientation in the unit cell used (by 0.09 eV relative to **X**, cf. Figure S11 and Table S1 of the Supporting Information) with an essentially flat geometry and an average distance of 2.74 Å to the topmost plane of the Cu(111) slab (Figure 3, **6 IS**). In contrast, in the biradical *meta*-aryne **6-2r** (which favors **Y** orientation by 0.16 eV) the σ -type dangling bonds bind to individual Cu atoms of the surface, pulling them out of the idealized Cu(111) lattice plane to some extent (Figure 3, **6-2r IS**). A similar geometry is observed for the corresponding biradical of DBOTP, see Figure S14 of the Supporting Information. The corresponding C-Cu bonds lead to a considerable tilting and deformation of the central phenylene ring, in agreement with the recently reported tilted geometry of a *meta*-aryne on Cu(111) revealed by nc-AFM.⁴⁶ Noteworthy, the current STM image of the MTP biradicals in Figure 1b do not allow to quantify such tilt due to limited resolution.

C-H bond breaking of **6** and **6-2r** (Scheme 2) are both endothermic reactions with corresponding energies of +1.06 eV and +0.33 eV (Figure 3), respectively. The crucial information to understand the experimental results lies in the comparison of the barriers for the activation of the target C-H bond in **6** and **6-2r**. C-H activation in intact **6** (in **Y** orientation) is associated with a calculated barrier of 1.80 eV. In comparison, the lowest C-H activation barrier for **6-2r** (0.97 eV, Table S3) is obtained when the target C-H group of **6-2r** is oriented along the **X** direction. For the calculation of the effective energy barrier, it has to be taken into account that the initial state **6-2r** prefers **Y** orientation by 0.16 eV (Figure 3 **6-2r IS**, and Table S1). Hence, the initially **Y** oriented **6-2r** has to reorient along **X** in order to reach the lowest-energy transition state, which has the target C-H bond parallel to **X** orientation (Figure 3, **6-2r TS**). This reorientation energy must be added to the direct C-H activation barrier along **X** according to the Curtin Hammett principle (assuming a negligible kinetic **X** \rightarrow **Y** reorientation barrier for **6-2r**), leading to an effective barrier for C-H activation **6-2r** \rightarrow **6-3r** of 1.13 eV. This activation barrier is substantially lower than that of intact **6** (1.80 eV) and is also in excellent agreement with the experimentally observed onset temperature for the dehydrogenative C-C coupling reaction (Scheme 1a). While the reduced activation barrier of the central C-H bond in the biradical **6-2r** is remarkable, note that **6-2r** alternatively could also be assumed to undergo a surface-assisted 1,2-hydrogen shift and subsequent C-C coupling to yield **2**. However, this reaction path, which is discussed in the SI (Scheme S1 and Figure S13), has a significantly higher activation barrier.

The difference of 0.67 eV in the activation barriers when starting from intact **6** as compared to *meta*-aryne **6-2r** can be understood qualitatively by inspecting the corresponding reactant species and transition structures shown in Figure 3: In the *meta*-aryne **6-2r**, the target C-H bond is pulled down close to the nearest Cu atom of the surface due to the strong binding of the adjacent two dangling bonds to the surface. In contrast, the corresponding C-H bond in intact **6** initially is much farther away from the copper surface at-

oms. Hence, the energetic effort (activation strain) to prepare the transition structure is expected to be larger for activation of intact **6** than for the *meta*-aryne **6-2r**. Therefore, the proximity of the target C-H bond to the Cu(111) surface reduces its dissociation barrier and hence leads to its selective activation. A similar case of C-H activation by proximity to a metal surface has also been reported for an *ortho*-aryne on Ag(111),⁴⁷ which to a certain extent weakens the C-H bond adjacent to the radical sites leading to the dehydrogenative coupling. This is qualitatively similar to metal-catalyzed C-H activation in solution. In this case, the directing group of the molecule anchors a single metal atom, which then facilitates the scission of the C-H bond nearest to it. In our case, however, the binding of the *meta*-aryne moiety to the Cu(111) surface is much more effective for facilitating C-H bond scission than the hypothetical binding to single copper atoms. This is supported by the calculated C-H bond dissociation energies for benzene C₆H₆ and 1,3-dicopper phenylene C₆H₄Cu₂ in the gas phase (no surface), which are computed to 4.96 and 4.52 eV (for C-H dissociation at the 2-position), respectively. Hence, the bonding of two single copper atom to the radicalic carbons of *meta*-aryne reduces the dissociation energy by only 9% for the enclosed C-H bond, compared to pristine benzene. This reduction is much less than that caused by the bonding of the *meta*-aryne to a copper surface discussed above, which reduces that barrier by 37%.

CONCLUSION

In summary, we have demonstrated the highly selective activation of the C-H bond between the two carbon radicals of *meta*-aryne chemisorbed on a Cu(111) surface. By using this approach, the selected precursor 4',6'-dibromo-*meta*-terphenyl **1** undergoes predominant dehydrogenative coupling into the 5',5''-diphenyl-*meta*-quaterphenyl biradical **2**. The precursor 3',5'-dibromo-*ortho*-terphenyl **3** forms 2,3,6,7,10,11-hexaphenyl-triphenylene **4** by a combination of Ullmann and dehydrogenative coupling. The mechanism for the considerable weakening of the target C-H bond in the *meta*-aryne has been revealed by density functional theory. It shows that extraordinary chemisorption of the *meta*-aryne on the Cu(111) surface leads to a close proximity of the target C-H group to the Cu(111) surface and a pronounced deformation of the phenyl ring. This effect reduces the dissociation energy of the target C-H bond by 37%. These findings provide insight into new approaches for the C-H bond activation of arenes, especially in the contexts of on-surface synthesis and heterogeneous catalysis.

METHODS

STM measurements were performed in an ultrahigh vacuum (UHV) system (base pressure 2×10^{-10} mbar) equipped with a SPECS STM Aarhus 150 STM and a photoelectron spectrometer with SPECS Phoibos 150 electron energy analyzer. All voltages refer to the sample, and the images were recorded in constant current mode. Moderate filtering (Gaussian smooth, background subtraction) has been

applied for noise reduction. The Cu(111) single crystal with an alignment of better than 0.1° relative to the nominal orientation were purchased from MaTecK, Germany. Preparation of a clean and well-defined Cu(111) surface was achieved by cycles of bombardment with Ar⁺ ions and annealing at 850 K. DBMTP and DBOTP were synthesized according to the literature (see the Supporting Information for details) and were evaporated in UHV from homebuilt Knudsen cells at 300 K.

The nc-AFM and several of the STM images (Figure 2a, b, c, and g) were recorded at 5 K in a low temperature (LT)-AFM/STM (Scienta Omicron, Germany) setup, with a base pressure below 1×10^{-10} mbar. AFM images were acquired by measuring the frequency shifts of a quartz tuning fork sensor in frequency modulation mode, at constant tip height and constant oscillation amplitude (resonance frequency about 27 kHz, Q-factor ≈ 20000 , PLL bandwidth of 10 Hz, scanning speed between 4 and 18 Å/s). An oscillation amplitude of 130 pm was used. The tungsten tip was functionalized with a single CO molecule using standard procedures. The molecules were evaporated using a homebuilt evaporation device.⁴⁸

Periodic density functional theory calculations of the DBMTP derivatives on Cu(111) were performed with the Vienna Ab Initio Simulation Package (VASP).⁴⁹ The PBE functional⁵⁰ was used in combination with the third-generation van der Waals dispersion correction due to Grimme (DFT-D₃)⁵¹ and the projector-augmented wave (PAW) ansatz⁵²⁻⁵³ for the atomic cores. A plane-wave cutoff energy of 400 eV was employed. The Cu(111) surface was modeled as a 3-layer, 7×8 copper atom slab in an orthorhombic unit cell. The corresponding lateral size of the unit cell is 17.67×17.49 Å², resulting in a separation of molecules in adjacent cells by at least 5 Å. A vacuum layer of at least 10 Å was introduced to isolate the repeated slabs from each other. Only the topmost layer was freely optimized together with the adsorbed molecules, while the bottom two Cu layers were kept frozen at their optimized bulk positions. A 2×2×1 Monkhorst-Pack k-point mesh was used in general. Geometries were optimized until the forces on the active atoms dropped below 5 meV/Å. Transition states were optimized with the improved dimer method (IDM).⁵⁴ Numerical vibrational frequency calculations on the transition structures to identify the search direction for the IDM method and to verify the nature of the stationary points found (one imaginary frequency) were carried out with all Cu positions of the slab frozen. Selected transition structures were further verified by steepest descent minimizations from starting structures which were slightly displaced from the corresponding transition state along the unstable mode to ensure that they indeed yield the desired reactant or product species. To further verify the results, additional calculations with a four-layer slab with both a 2×2×1 (single-point energies for transition states, other geometries optimized) and a 4×4×1 k-point mesh (all single-point energies, *i.e.*, no geometry optimizations) were carried out and resulted in essentially the same relative energies to within 0.1 eV. Turbomole RI-DFT calculations for benzene C₆H₆ and 1,3-dicopper phenylene in the gas phase

were performed using the PBE functional and the def2-TZVP basis set.⁵⁵⁻⁵⁶

ASSOCIATED CONTENT

Supporting Information. The Supporting Information is available free of charge on the ACS Publications website. Precursor synthesis and characterization, structure analysis and yield statistics of the products, and additional data and details of the DFT calculations.

AUTHOR INFORMATION

Corresponding Authors

* andre.schirmeisen@ap.physik.uni-giessen.de

* gerhard.hilt@uni-oldenburg.de

* wolfgang.hieringer@fau.de

* michael.gottfried@chemie.uni-marburg.de

Author Contributions

‡ Q. F. and S. W. contributed equally.

Notes

The authors declare no competing financial interest.

ACKNOWLEDGMENT

Financial support by the Deutsche Forschungsgemeinschaft via the grants GO 1812/2-1 and HI 655/18-1, the CRC 1083, the Cluster of Excellence EXC 315 "Engineering of Advanced Materials", and the GRK (Research Training Group) 2204 "Substitute Materials for Sustainable Energy Technologies" is gratefully acknowledged. This project was also supported by the Laboratory of Materials Research (LaMa) of JLU and the LOEWE program of excellence of the Federal State of Hessen (project initiative STORE-E). The RRZE of the University of Erlangen-Nürnberg is acknowledged for computational resources. Q.T.F thanks the Alexander von Humboldt-Foundation for a Research Fellowship for Postdoctoral Researchers.

REFERENCES

- Ball, L. T.; Lloyd-Jones, G. C.; Russell, C. A. *Science* **2012**, *337*, 1644-1648.
- Yang, J. *Org. Biomol. Chem.* **2015**, *13*, 1930-1941.
- Boorman, T. C.; Larrosa, I. *Chem. Soc. Rev.* **2011**, *40*, 1910-1925.
- Davies, H. M. L.; Du Bois, J.; Yu, J. Q. *Chem. Soc. Rev.* **2011**, *40*, 1855-1856.
- McMurray, L.; O'Hara, F.; Gaunt, M. J. *Chem. Soc. Rev.* **2011**, *40*, 1885-1898.
- Cui, X.; Mo, J.; Wang, L.; Liu, Y. *Synthesis* **2015**, *47*, 439-459.
- Chen, D. Y. K.; Youn, S. W. *Chem. Eur. J.* **2012**, *18*, 9452-9474.
- Kakiuchi, F.; Kan, S.; Igi, K.; Chatani, N.; Murai, S. *J. Am. Chem. Soc.* **2003**, *125*, 1698-1699.
- Murai, S.; Kakiuchi, F.; Sekine, S.; Tanaka, Y.; Kamatani, A.; Sonoda, M.; Chatani, N. *Nature* **1993**, *366*, 529-531.
- Davies, H. M.; Morton, D. *J. Org. Chem.* **2016**, *81*, 343-350.
- Kinuta, H.; Tobisu, M.; Chatani, N. *J. Am. Chem. Soc.* **2015**, *137*, 1593-1600.
- Zhang, F.; Spring, D. R. *Chem. Soc. Rev.* **2014**, *43*, 6906-6919.
- Engle, K. M.; Mei, T.-S.; Wasa, M.; Yu, J.-Q. *Acc. Chem. Res.* **2012**, *45*, 788-802.
- Fan, Q.; Gottfried, J. M.; Zhu, J. *Acc. Chem. Res.* **2015**, *48*, 2484-2494.

15. Cai, J.; Ruffieux, P.; Jaafar, R.; Bieri, M.; Braun, T.; Blankenburg, S.; Muoth, M.; Seitsonen, A. P.; Saleh, M.; Feng, X.; Müllen, K.; Fasel, R. *Nature* **2010**, *466*, 470-473.
16. Talirz, L.; Ruffieux, P.; Fasel, R. *Adv. Mater.* **2016**, *28*, 6222-6231.
17. Ruffieux, P.; Wang, S.; Yang, B.; Sánchez-Sánchez, C.; Liu, J.; Dienel, T.; Talirz, L.; Shinde, P.; Pignedoli, C. A.; Passerone, D.; Dumslaff, T.; Feng, X.; Müllen, K.; Fasel, R. *Nature* **2016**, *531*, 489-492.
18. Cai, J.; Pignedoli, C. A.; Talirz, L.; Ruffieux, P.; Sode, H.; Liang, L.; Meunier, V.; Berger, R.; Li, R.; Feng, X.; Müllen, K.; Fasel, R. *Nat. Nanotechnol.* **2014**, *9*, 896-900.
19. Treier, M.; Pignedoli, C. A.; Laino, T.; Rieger, R.; Müllen, K.; Passerone, D.; Fasel, R. *Nat. Chem.* **2011**, *3*, 61-67.
20. Rogers, C.; Chen, C.; Pedramrazi, Z.; Omrani, A. A.; Tsai, H. Z.; Jung, H. S.; Lin, S.; Crommie, M. F.; Fischer, F. R. *Angew. Chem. Int. Ed.* **2015**, *54*, 15143-15146.
21. Jacobse, P. H.; van den Hoogenband, A.; Moret, M. E.; Klein Gebbink, R. J.; Swart, I. *Angew. Chem. Int. Ed.* **2016**, *55*, 13052-13055.
22. Otero, G.; Biddau, G.; Sanchez-Sanchez, C.; Caillard, R.; Lopez, M. F.; Rogero, C.; Palomares, F. J.; Cabello, N.; Basanta, M. A.; Ortega, J.; Mendez, J.; Echavarren, A. M.; Perez, R.; Gomez-Lor, B.; Martin-Gago, J. A. *Nature* **2008**, *454*, 865-868.
23. Sanchez-Valencia, J. R.; Dienel, T.; Groning, O.; Shorubalko, I.; Müller, A.; Jansen, M.; Amsharov, K.; Ruffieux, P.; Fasel, R. *Nature* **2014**, *512*, 61-64.
24. de Oteyza, D. G.; Garcia-Lekue, A.; Vilas-Varela, M.; Merino-Diez, N.; Carbonell-Sanroma, E.; Corso, M.; Vasseur, G.; Rogero, C.; Guitian, E.; Pascual, J. I.; Ortega, J. E.; Wakayama, Y.; Pena, D. *ACS Nano* **2016**, *10*, 9000-9008.
25. Schulz, F.; Jacobse, P. H.; Canova, F. F.; van der Lit, J.; Gao, D. Z.; van den Hoogenband, A.; Han, P.; Klein Gebbink, R. J. M.; Moret, M.-E.; Joensuu, P. M.; Swart, I.; Liljeroth, P. *J. Phys. Chem. C* **2017**, *121*, 2896-2904.
26. Sun, Q.; Zhang, C.; Cai, L.; Xie, L.; Tan, Q.; Xu, W. *Chem. Commun.* **2015**, *51*, 2836-2839.
27. Sun, Q.; Zhang, C.; Kong, H.; Tan, Q.; Xu, W. *Chem. Commun.* **2014**, *50*, 11825-11828.
28. Han, P.; Akagi, K.; Federici Canova, F.; Mutoh, H.; Shiraki, S.; Iwaya, K.; Weiss, P. S.; Asao, N.; Hitosugi, T. *ACS Nano* **2014**, *8*, 9181-9187.
29. Li, Q.; Yang, B.; Lin, H.; Aghdassi, N.; Miao, K.; Zhang, J.; Zhang, H.; Li, Y.; Duhm, S.; Fan, J.; Chi, L. *J. Am. Chem. Soc.* **2016**, *138*, 2809-2814.
30. Wang, C. X.; Jin, Q.; Shu, C. H.; Hua, X.; Long, Y. T.; Liu, P. N. *Chem. Commun.* **2017**, *53*, 6347-6350.
31. Kocic, N.; Liu, X.; Chen, S.; Decurtins, S.; Krejci, O.; Jelinek, P.; Repp, J.; Liu, S. X. *J. Am. Chem. Soc.* **2016**, *138*, 5585-5593.
32. Fan, Q.; Wang, C.; Han, Y.; Zhu, J.; Kuttner, J.; Hilt, G.; Gottfried, J. M. *ACS Nano* **2014**, *8*, 709-718.
33. Wang, W. H.; Shi, X. Q.; Wang, S. Y.; Van Hove, M. A.; Lin, N. *J. Am. Chem. Soc.* **2011**, *133*, 13264-13267.
34. Chen, M.; Xiao, J.; Steinrück, H.-P.; Wang, S.; Wang, W.; Lin, N.; Hieringer, W.; Gottfried, J. M. *J. Phys. Chem. C* **2014**, *118*, 6820-6830.
35. Fan, Q.; Wang, C.; Han, Y.; Zhu, J.; Hieringer, W.; Kuttner, J.; Hilt, G.; Gottfried, J. M. *Angew. Chem. Int. Ed.* **2013**, *52*, 4668-4672.
36. Fan, Q.; Wang, T.; Dai, J.; Kuttner, J.; Hilt, G.; Gottfried, J. M.; Zhu, J. *ACS Nano* **2017**, *11*, 5070-5079.
37. Zint, S.; Ebeling, D.; Schlöder, T.; Ahles, S.; Mollenhauer, D.; Wegner, H. A.; Schirmeisen, A. *ACS Nano* **2017**, *11*, 4183-4190.
38. Rastgoo Lahrood, A.; Björk, J.; Heckl, W. M.; Lackinger, M. *Chem. Commun.* **2015**, *51*, 13301-13304.
39. Pavlicek, N.; Mistry, A.; Majzik, Z.; Moll, N.; Meyer, G.; Fox, D. J.; Gross, L. *Nat. Nanotechnol.* **2017**, *12*, 308-311.
40. Cirera, B.; Björk, J.; Otero, R.; Gallego, J. M.; Miranda, R.; Eciija, D. *J. Phys. Chem. C* **2017**, *121*, 8033-8041.
41. Simonov, K. A.; Vinogradov, N. A.; Vinogradov, A. S.; Generalov, A. V.; Zagrebina, E. M.; Svirskiy, G. I.; Cafolla, A. A.; Carpy, T.; Cuniffe, J. P.; Taketsugu, T.; Lyalin, A.; Mårtensson, N.; Preobrajenski, A. B. *ACS Nano* **2015**, *9*, 8997-9011.
42. Kawai, S.; Takahashi, K.; Ito, S.; Pawlak, R.; Meier, T.; Spijker, P.; Canova, F. F.; Tracey, J.; Nozaki, K.; Foster, A. S.; Meyer, E. *ACS Nano* **2017**, *11*, 8122-8130.
43. Shaik, J. B.; Ramkumar, V.; Varghese, B.; Sankararaman, S. *Beilstein J. Org. Chem.* **2013**, *9*, 698-704.
44. Romero, C.; Peña, D.; Pérez, D.; Guitián, E. *Chem. Eur. J.* **2006**, *12*, 5677-5684.
45. Yatabe, T.; Harbison, M. A.; Brand, J. D.; Wagner, M.; Müllen, K.; Samori, P.; Rabe, J. P. *J. Mater. Chem.* **2000**, *10*, 1519-1525.
46. Pavlicek, N.; Majzik, Z.; Collazos, S.; Meyer, G.; Perez, D.; Guitian, E.; Pena, D.; Gross, L. *ACS Nano* **2017**, *11*, 10768-10773.
47. Sanchez-Sanchez, C.; Nicolai, A.; Rossel, F.; Cai, J.; Liu, J.; Feng, X.; Müllen, K.; Ruffieux, P.; Fasel, R.; Meunier, V. *J. Am. Chem. Soc.* **2017**, *139*, 17617-17623.
48. Zint, S.; Ebeling, D.; Ahles, S.; Wegner, H. A.; Schirmeisen, A. *J. Phys. Chem. C* **2016**, *120*, 1615-1622.
49. Kresse, G.; Furthmüller, J.; Hafner, J. Vienna Ab Initio Simulation Package (VASP), version 5.3.5; www.vasp.at.
50. Perdew, J. P.; Burke, K.; Ernzerhoff, M. *Phys. Rev. Lett.* **1996**, *7*, 3865.
51. Grimme, S.; Antony, J.; Ehrlich, S.; Krieg, H. *J. Chem. Phys.* **2010**, *132*, 154104.
52. Blöchl, P. E. *Phys. Rev. B* **1994**, *50*, 17953-17979.
53. Kresse, G.; Joubert, D. *Phys. Rev. B* **1999**, *59*, 1758-1775.
54. Heyden, A.; Bell, A. T.; Keil, F. J. *J. Chem. Phys.* **2005**, *123*, 224101.
55. Ahlrichs, R.; Furche, F.; Hättig, C.; Klopper, W. M.; Sierka, M.; Weigend, F. Turbomole program package, version 6.6, Karlsruhe, Germany, since 1989 (<http://www.turbomole.com>).
56. Weigend, F.; Ahlrichs, R. *Phys. Chem. Chem. Phys.* **2005**, *7*, 3297-3305.

Table of Contents

